

Research Paper

Analysis of Ferrohydrodynamic Interaction in Unsteady Nanofluid Flow over a Curved Stretching Sheet with Melting Heat Peripheral Conditions

A.M. Obalalu¹, Adil Darvesh², A.O. Akindele³, Amanullah Phulpoto⁴, A.D. Adeshola⁵, M. Asif Memon⁴

¹ Department of Mathematical Sciences, Augustine University Ilara-Epe, Lagos, Nigeria, Email: adebowale.obalalu17@gmail.com

² Department of Mathematics and statistics Hazara University Mansehra, 21300 Pakistan, Email: adildarvesh@hu.edu.pk

³ Department of Pure and Applied Mathematics, Ladoke Akintola University of Technology, Nigeria, Email: aoakindele65@pgschool.lautech.edu.ng

⁴ Department of Mathematics and Social Sciences, Sukkur IBA University, Sukkur, 65200, Sindh, Pakistan,
Email: amanullah@iba-suk.edu.pk (A.P); asif-memon@iba-suk.edu.pk (M.A.M.)

⁵ Department of Mathematics and Statistics, Kwara State University, Malete, Nigeria, Email: adeshola.dauda@kwasu.edu.ng

Received January 15 2024; Revised May 10 2024; Accepted for publication May 15 2024.

Corresponding author: M. Asif Memon (asif-memon@iba-suk.edu.pk)

© 2024 Published by Shahid Chamran University of Ahvaz

Abstract. Studying the impact of Ferrohydrodynamic interaction on the flow of Casson-Williamson nanofluid present a significant insight into complex fluid behaviour in several fields including aerospace engineering, energy systems, drug delivery, chemical engineering, and various industries. Owing to its usage, current investigation deals with effect of magnetic dipole on the time-based unsteady nanofluid flow of homogeneous and heterogeneous reaction driven by a curved stretching sheet with slip and melting heat boundary conditions. This research predicts the optimal ranges of parameters for achieving higher heat transport performance by studying the Cattaneo-Christov heat flux model and an exponential heat source. The governing equations are converted into dimensionless form by employing suitable similarity transformations. The Galerkin-weighted residual technique is used to numerically solve the resulting non-dimensional equations with the assistance of the MATHEMATICA 11.3 software. The outcome indicates that the thermal buoyancy parameter significantly enhances fluid motion, while the thermal radiation parameter reduces the fluid temperature. This outcome greatly influences the prospective uses of Ferrohydrodynamic interaction in enhancing heat and mass transport in nanofluid cooling systems.

Keywords: Casson-Williamson nanofluid; Heterogeneous reaction; Cattaneo-Christov heat flux.

1. Introduction

The extraordinary characteristics of nanofluids enhance their ability to transfer heat effectively. Nanofluids can enhance the efficacy of heat and energy transfer in various devices and several other things. Temperature significantly impacts the conductivity of nanofluids, rendering them superior to regular fluids in heat conduction, particularly at low concentrations. This factor contributes practically to numerous circumstances due to its excellent ability to retain heat. Wen et al. [1] studied nanofluid for detail analysis of heat transfer applications and made significant views. Creating, examining, and measuring the ability of nanofluids to conduct heat is a common matter in many problems. Wu et al. [2] studied the ability of nanofluids in heat conduction and presented its significance in several issues such as fabrication analysis and measurement. Later, an investigation made by Saidur et al. [3] to examine the usage and obstacles in implementing nanofluids. Many researchers studied nanofluids for heat transfer and discussed several real-life examples. Research has been conducted by Bhagore et al. [4], on the utilization of nanofluids as a cooling agent in automotive radiators, along with the challenges associated with their implementation. Sajid et al. [5] made a new development in heat transfer devices using different tiny particles. The thermal conductivity of a material can be greatly enhanced through different factors. Younes et al. [6] discussed some important facts of nanofluids and presented their benefits in many applications. Nagaraja et al. [7] studied the heat transfer using Casson fluid with sodium alginate nanocomposites over a Riga geometry. The study focused the thermal performance of the Casson nanofluid due to immersion of these nanocomposite. The result of the study revealed that the synthesized Casson nanofluid is good in heat transport. An approach to combat global warming was given by Darvesh et al. [8]. This study involves the application of nanofluid, which consists of a combination of nano particles suspended in a liquid, while considering the influences of chemical processes and radiation on magnetohydrodynamics. Madhukesh et al. [9] discussed microchannel flow using computational study. they studied the fluid flow containing three distinct



particles and influenced by a discharge concentration and non-uniform heat source. Furthermore, in [10], they used the Riga surface in presence of thermal radiation and discussed the effectiveness and crucial role magnetized nanoparticle aggregation in a conventional fluid. The Al_2O_3 nanoparticles were taken in the base fluid (water) to observe this mechanism. Figure 1 depicts several significant real-world applications of nanofluids [11].

Rheological properties of Casson fluid can facilitate the comprehension of the flow behaviour of viscous-elastic fluids. The model smoothly shifts from a Newtonian state to the Yield region. The viscosity of a Casson-Williamson decreases as it is stirred or moved while it exhibit an extremely thick behaviour and adhesive nature when in a state of rest. Moreover, there is a distinct point at which it initiates flowing and, on another point, where it thins out significantly under intense stirring. Concentrated fruit juices, Honey, Jellies, and sauce of tomato are all familiar examples of substances that exhibit the properties of Casson fluid. Casson-Williamson fluid possesses a distinctive characteristic known as yield stress. Industries that operate with polymers and the field of biomechanics is also highly dependent on this significant aspect. The study conducted by Yousef et al. [9] investigated the effects of a chemical reaction on the flow of a Williamson Casson nanofluid over a slippery stretching sheet through a porous medium. The effects of chemical reactions and heat radiation on the flow of a Casson-Williamson nanofluid over a stretching surface were studied by Humane et al. [10]. Mangathai et al. [14] discussed that radiation and dissipation of viscosity can cause an irregular movement in Williamson and Casson nano fluid. Later research was conducted by Salawu et al. [15] to compare the flow of nanofluids around a flat plate using a method called spectral quasi-linearization. The study focused on how different fluids behave in three-dimensional flow conditions. Olayemi et al. [16] focused on understanding the heat and mass transfer mechanisms that take place when a cylinder, subjected to vertical motion, interacts with a specific type of fluid called a Casson-Williamson nanofluid. Madhukesh et al. [17] used non-Fourier heat flux model and made the numerical simulation of hybrid nanofluid along a curved sheet influenced by Newtonian heat source. Kumar et al. [18] discussed the buoyancy force in the flow of unsteady Casson-Williamson nanofluid over a stretching slippery curved in presence of heat source and analysed the Magnetic dipole effects. Falodun et al. [19] made a detail study of boundary layer flow of Casson-Williamson nanofluids with Soret-Dufour phenomenon for the analysis of linear and quadratic multiple regressions. Obalalu et al. [20] discussed the radiative Casson nanofluid over a Riga surface for energy generation through minimization on electromagnetohydrodynamic. Furthermore in [21] he studied the heat transfer and electromagnetohydrodynamic and analysed the use of nanomaterial fluid flow in in solar energy. Many more studies have been conducted by researchers and scholars around the globe. A few examples are listed in references [22-29].

Magnetic nanoparticles display distinctive behaviour and possess exceptional magnetic characteristics when in suspension. To modulate fluidity, it is essential to primarily focus on weak magnetic effects for observing flow behaviour. This phenomenon is useful to study the different key properties of fluid flow. Due to magnetic control phenomenon various facts can be explored and many developments can be carried out in numerous medical, engineering, and technical applications. A lot of studies have been carried out in this regard. Odenbach et al. [30] studied the magnetic dipoles effects produced by magnetic suspension of nanoparticles in a base fluid and provide some moving gasps of nanoparticles. The findings revealed that mixture of minuscule magnetic nanoparticles can be manipulated by magnet. Wang et al. [31] studied the behaviour of magnetic dipole by assuming different boundary conditions on the fluid. The research stated that magnetic dipole can be affected by different boundaries conditions and equilibrium conditions may also be distorted by different fluctuations. The study of magnetic dipole for the viscous ferro fluid with thermal radiated effects over a stretching surface was presented by Zeeshan et al. [32]. Later several facts are also explored by studying Jeffery fluid flow over a stretching Surface for examination of transferring heat in the presence of magnetic dipole injection-suction effects in [33]. Darvesh et al. [34] study the cross-fluid flow over a three directional stretching surface under the influence of magnetic dipole to characterize the high and shear rate of nanofluid flow, by using cross mathematical modelling under the influence of magnetic dipole. Moreover, numerous studies have been conducted by many researchers looking at different role of magnetic dipole with different assumptions and captivating fluid flow behaviour in many complex situations a few of vital research papers are [35-38].

The transmission of thermal energy among two entities or within an object is a vital occurrence in the realm of nature. To grasp the mechanics of Fourier's classical heat conduction law, Cattaneo et al. [39] devised a means of measuring the rate at which heat can be dissipated. Han et al. [40] used "Cattaneo Christov" model of heat-Flux for couple fluid flow together with heat transfer effects in a viscous fluid. To observe the impact of the heat flux by Cattaneo Christov for a fluid flow with variated thermal conductivity over a thick surface and a novel three-dimensional flow phenomenon of mass diffusivity as well as heat conduction was described was studied by Hayyat et al. [41]. In this study OHAM strategy was utilized for the analytical solutions of model equations. Later, Khan et al. [42] the Cattaneo Christov heat flux model is used to study the same flow systems in burgers fluid for the heat transfer rate. Recently Cattaneo-Christov heat flux model for the boundary layer flow together with heat transfer rate due to thermal radiation effect have been extensively investigated in many literatures [43-49].



Fig. 1. Physical applications of nanofluids.



Buoyancy forces together with Cattaneo Christov model of Heat Flux was mainly considered by many scientists in the study of Casson Williamson nanofluids flow based on unsteadiness conditions over different curved geometries. Their simulations also included many captivating features such as joule heating effects, thermal radiations homo heterogeneous consequences, exponential heat sources and melting heat peripheral conditions. Shankar et al. [50] characterized the chaotic dynamics of fluidity. The distribution of the heat source was unevenly applied to analyses the unpredictable movements of heat and liquid particles in a flowing nanofluid over a surface undergoing stretching. A numerical study conducted by Ramzan et al. [51] for Williamson fluid flow behaviour in the presence of Cattaneo Christov and magnetohydrodynamic stagnation by assuming convective boundary conditions and homo-heterogeneous reactions. Melting phenomenon of nanofluid together with thermal aspects on stretching-Sheet in unsteady situation was characterized by Kumar et al. [52]. Upadhyya et al. [53] discussed micro nanofluid with Cattaneo Christov model for nonlinear system governing sets of equations-based unsteadiness convection. The study on Williamson fluid flow over a flat type of surface with variable heat sink source in the presence of MHD effects was also conducted by Kumar et al. [54]. Many other of magneto hydrodynamics substantial implications for numerous engineering purposes and the role of Cattaneo Christov model of Heat Flux in the realm of fluid flow for many industrial innovations were examined in [55-60].

1.1. Aims and novelty of current work

This study incorporates advanced modelling approaches with a thorough analysis of physical occurrences, providing insights into the magnetic dipole nanofluid flows influenced by numerous features. The study of the recent literature exhibits that the current study, which simulates the unsteady flow of Ferrohydrodynamic interaction is innovative and the combination of Cattaneo-Christov heat flux model with buoyancy effect has significant applications in the industrial sector. The presence of the Cattaneo-Christov heat flux model into the numerical simulation distinguishes this present work from past research studies. This research model allows a more accurate illustration of thermal conduction in magnetic dipole nanofluid flows, specifically when studying the curved stretching sheet. This novel approach substantially increases the accuracy of heat transport rate. The study includes several physical phenomena such as homo-heterogenic reactions, Casson-Williamson nanofluid, melting heat and slip boundary conditions.

1.2. Applications of Magnetic dipole Nanofluids

The use of magnetic dipoles can be employed to regulate the speed flow and thermal transport characteristics of nanofluids. This has substantial implications for numerous engineering purposes, such as nanofluid heat transport, electromagnetic Motors, and Generators, magnetohydrodynamic (MHD) pumps, drug discovery and development: and microfluidic devices. The results of this research highlight the potential advantages of employing magnetic dipoles in these applications.

1.3. Motivation

This comprehensive research objectives are to solve the difficulties of a multifaceted system, provide theoretical understandings, and contribute to scientific and industrial progresses. By considering numerous factors and applying numerical simulations to examines their properties, this study assists as a valuable endeavour with implications for various applications.

The research questions are:

- What is the significance of incorporating the Cattaneo-Christov heat flux model and exponential heat source in predicting optimal parameter ranges for heat transport performance?
- How do homogeneous and heterogeneous reactions impact the flow behaviour?
- How do the outcomes of the study contribute to the field of fluid dynamics, especially in terms of thermal buoyancy and thermal radiation parameters?
- Why were the Galerkin-weighted residual technique chosen for numerical solutions, and how does the use of MATHEMATICA 11.3 software enhance the reliability of the results?
- How do slip and melting heat boundary conditions contribute to the overall understanding of the nanofluid flow on a curved stretching sheet?

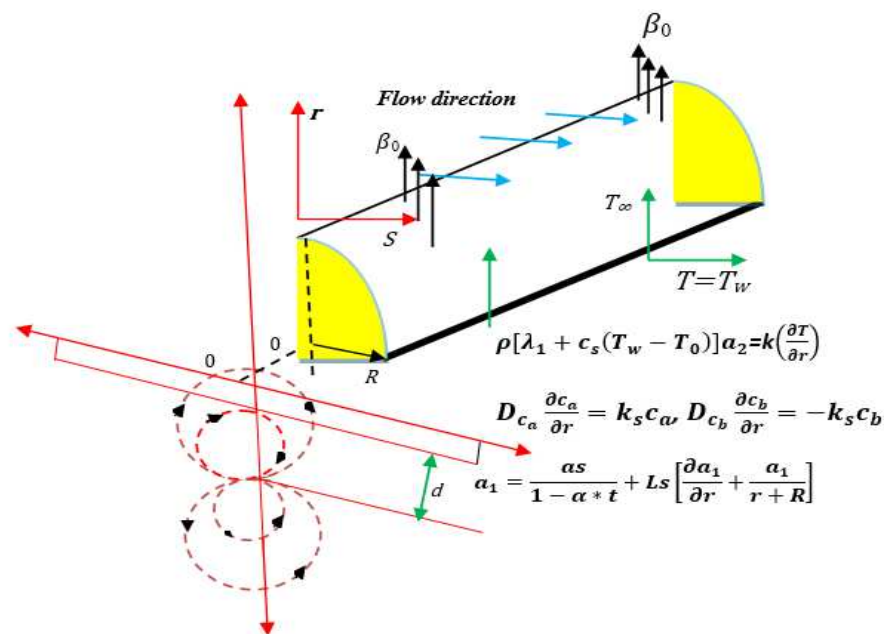


Fig. 2. Schematic diagram of the problem.



2. Mathematical Model of the Problem

As presented in Fig. 2, the sheet is stretched around a semicircle with a radius R when equal and opposite pressures are applied along the s -orientation, while keeping the origin still and the r -orientation perpendicular to it. Considering the unsteady nature of the flow, we consider the behaviour of Casson-Williamson nanofluid along a curved stretching sheet. We base our analysis on the following assumptions in this case:

- The magnetic field $\beta_m = \frac{B_0}{\sqrt{(1-\alpha^*t)}}$ is applied in the R direction when considering the influence of the magnetic dipole moment on fluid flow.
- The stretching speed of the sheet can be represented by $U_w(s) = \frac{a}{1-\alpha^*t}$ where a, α^* and t are stretching rate, constant with dimension reciprocal of time constant and time, respectively.
- The slippery condition assists in improving the boundary of the melting surface.
- Two chemical samples A and B are studied for their homo-heterogenic reactions to explain the mass transfer operation. The corresponding concentrations C_a and C_b are analysed to understand this process thoroughly. The reaction $A+2B \rightarrow 3B$ occurs homogeneously on the carrier surface at a rate of $k_c C_a C_b^2$, while the reaction $A \rightarrow B$ occurs heterogeneously at a certain rate of $k_s C_a$.
- The effect of buoyancy is considered to investigate the flow characteristics of the nanofluid.
- The energy equation incorporates the effects of Cattaneo-Christov heat flux model and an exponential space-dependent heat source to investigate the heat performance of the flow.

2.1. Governing equations

Under the assumptions, the boundary layer approximation can be expressed as [18]:

$$\frac{\partial}{\partial r} \{ (R+r)a_2 \} + R \frac{\partial a_1}{\partial s} = 0, \tag{1}$$

$$\frac{\rho}{r+R} a_1^2 = \frac{\partial p}{\partial r}, \tag{2}$$

$$\frac{\partial a_1}{\partial t} + a_2 \frac{\partial a_1}{\partial r} + \frac{R}{r+R} a_1 \frac{\partial a_1}{\partial s} + \frac{a_1 a_2}{r+R} = -\frac{R}{\rho(r+R)} \frac{\partial p}{\partial s} + a_2 \left[\left(1 + \frac{1}{\beta}\right) \left(\frac{\partial^2 a_1}{\partial r^2} + \frac{1}{r+R} \frac{\partial a_1}{\partial r} - \frac{a_1}{(r+R)^2} \right) \sqrt{2\Gamma} \left\{ \frac{\partial a_1}{\partial r} \frac{\partial^2 a_1}{\partial r^2} + \frac{1}{r+R} \left\{ \left(\frac{\partial a_1}{\partial r} \right)^2 - a_1 \frac{\partial^2 a_1}{\partial r^2} \right\} + \frac{a_1^2}{(r+R)^3} \right\} - \frac{2a_1}{(r+R)^2} \frac{\partial a_1}{\partial r} \right] + \frac{\mu_0 M}{\rho} \frac{\partial H}{\partial s} + g[\beta_T(T - T_\infty)] - \frac{\sigma}{\rho} B_m^2 a_1, \tag{3}$$

$$\frac{\partial T}{\partial t} + a_2 \frac{\partial T}{\partial r} + \frac{R}{r+R} \frac{\partial T}{\partial s} = \alpha \left(\frac{\partial^2 T}{\partial r^2} + \frac{1}{r+R} \frac{\partial T}{\partial r} \right) + \tau \left[D_{C_a} \left(\frac{\partial C_a}{\partial r} \frac{\partial T}{\partial r} \right) + \frac{D_T}{T_\infty} \left(\frac{\partial T}{\partial r} \right)^2 \right] - \frac{1}{\rho c_p} \frac{1}{r+R} \frac{\partial [(r+R)q_r]}{\partial r} + \frac{Q_0}{\rho c_p} (T - T_\infty) e^{-\sqrt{\frac{\sigma}{2\Gamma}} r} + \frac{1}{\rho c_p} \left[a_1 \frac{\partial H}{\partial s} + \frac{\partial H}{\partial r} \right] \mu_0 T \frac{\partial M}{\partial T} - \lambda_1 \left[a_2^2 \frac{\partial^2 T}{\partial r^2} + a_1^2 \left(\frac{R}{r+R} \right)^2 \frac{\partial^2 T}{\partial s^2} + (a_2 \frac{\partial a_2}{\partial r} + \frac{a_1 R}{r+R} \frac{\partial a_2}{\partial s}) \frac{\partial T}{\partial s} + \left(\frac{a_2 R}{r+R} \frac{\partial a_1}{\partial r} + a_1^2 \left(\frac{R}{r+R} \right)^2 \frac{\partial a_1}{\partial s} \right) \frac{\partial T}{\partial s} + \frac{2a_1 a_2 R}{r+R} \frac{\partial^2 T}{\partial r \partial s} \right] + \frac{\sigma}{\rho c_p} B_m^2 a_1^2, \tag{4}$$

$$\frac{\partial C_a}{\partial t} + a_2 \frac{\partial C_a}{\partial r} + \frac{R a_1}{r+R} \frac{\partial C_a}{\partial s} = D_{C_a} \left(\frac{\partial^2 C_a}{\partial r^2} + \frac{1}{r+R} \frac{\partial C_a}{\partial r} \right) + \frac{D_T}{T_\infty} \left(\frac{\partial^2 T}{\partial r^2} + \frac{1}{r+R} \frac{\partial T}{\partial r} \right) - k_c C_a C_b^2, \tag{5}$$

$$\frac{\partial C_b}{\partial t} + a_2 \frac{\partial C_b}{\partial r} + \frac{R a_1}{r+R} \frac{\partial C_b}{\partial s} = D_{C_b} \left(\frac{\partial^2 C_b}{\partial r^2} + \frac{1}{r+R} \frac{\partial C_b}{\partial r} \right) + \frac{D_T}{T_\infty} \left(\frac{\partial^2 T}{\partial r^2} + \frac{1}{r+R} \frac{\partial T}{\partial r} \right) + k_c C_a C_b^2, \tag{6}$$

with the following boundary conditions (BCs) [32]:

$$a_1 = \frac{as}{(1-\alpha^*t)} + Ls \left[\frac{\partial a_1}{\partial r} + \frac{a_1}{r+R} \right], \quad k \left(\frac{\partial T}{\partial r} \right) = \rho[\lambda_1 + c_s(T_m - T_0)]a_2, \tag{7}$$

$$T = T_w, \quad D_{C_a} \frac{\partial C_a}{\partial r} = k_s C_a, \quad D_{C_b} \frac{\partial C_b}{\partial r} = -k_s C_a$$

$$\text{at } r = 0, \quad a_1 \rightarrow 0, a_2 \rightarrow 0, \frac{\partial a_1}{\partial r} \rightarrow 0, T \rightarrow T_\infty, C_a \rightarrow C_0, C_b \rightarrow 0 \text{ as } r \rightarrow \infty.$$

2.2. Magnetic dipole effect

The effects on the liquid stream are due to the magnetic field caused by the apparent magnetic dipole and its scalar strength Φ . These effects can be summarized as follows:

$$\Phi = \frac{\gamma}{2\pi} \left\{ \frac{s}{s^2 + (r+d)^2} \right\}, \tag{8}$$

The associated magnetic field H shows the following properties:

$$H_r = \frac{\partial \Phi}{\partial r} = \frac{\gamma}{2\pi} \frac{2s(r+d)}{\{s^2 + (r+d)^2\}^2}, \tag{9}$$

$$H_s = \frac{\partial \Phi}{\partial s} = \frac{\gamma}{2\pi} \frac{s^2 - (r+d)}{\{s^2 + (r+d)^2\}^2}, \tag{10}$$

This relation shows the quantity of H as a direct variation of the magnetic force:

$$H = \sqrt{H_r^2 + H_s^2}. \tag{11}$$

A linear relationship exists between temperature T and magnetization M , as depicted below:



$$M = K_1(T - T_\infty), \tag{12}$$

2.3. Thermal radiation effect

Given by the Rosseland estimation, the radiative heat flow is:

$$q_r = -\frac{4\sigma^* \partial T^4}{3k^* \partial r} = -\frac{16\sigma^* T_\infty^3 \partial T}{3k^* \partial r}, \tag{13}$$

2.4. Transformed Equations

The following morphing catalysts are explored to understand the simplified form of flow steering equations [20].

$$\begin{aligned} a_1 &= \frac{as}{(1 - \alpha^*t)} w'(\eta), & a_2 &= \frac{-R}{r + R} \sqrt{\frac{aa_2}{(1 - \alpha^*t)}} w(\eta), \\ \eta &= \sqrt{\frac{a}{a_2(1 - \alpha^*t)}} r, & p &= \frac{\rho a^2 s^2}{(1 - \alpha^*t)^2} P(\eta), \\ k &= \sqrt{\frac{a}{a_2(1 - \alpha^*t)}} R, & \theta &= \frac{T - T_\infty}{T_w - T_\infty}, C_a = C_0 C_1(\eta), C_b = C_0 C_2(\eta), \end{aligned} \tag{14}$$

Expression (1) is identically verified and Eqs. (2) to (5) become

$$\frac{\partial p}{\partial \eta} = \frac{w'^2}{\eta + \kappa}, \tag{15}$$

$$\begin{aligned} \frac{2\kappa}{\eta + \kappa} P &= \frac{\kappa}{(\eta + \kappa)^2} w w' + \frac{\kappa}{\eta + \kappa} w w'' - \frac{\kappa}{\eta + \kappa} w w'^2 + \left(1 + \frac{1}{\beta}\right) \left[w''' + \frac{1}{(\eta + \kappa)} w'' - \frac{1}{(\eta + \kappa)^2} w' \right] \\ &+ We \left[w'' w''' + \frac{1}{(\eta + \kappa)} (w''^2 - w' w''') - \frac{2w' w''}{(\eta + \kappa)^2} + \frac{w'^2}{(\eta + \kappa)^3} \right] - \delta^* \left[w' + \frac{\eta}{2} w'' \right] - \frac{2\beta_m}{(n + b)^4} \theta + \lambda_T \theta - M^* w', \end{aligned} \tag{16}$$

$$\begin{aligned} \frac{1}{P_r} [1 + Rd] \left(\frac{1}{(\eta + \kappa)} \theta' + \theta'' \right) &+ \frac{\kappa}{\eta + \kappa} w \theta' + Nb C_1' \theta' + Nt \theta'^2 - \frac{\eta}{2} \delta^* \theta' + Ec M^* w'^2 + Q \theta e^{-n} - C_H \left(\frac{\kappa}{\eta + \kappa} \right)^2 \left[w^2 \theta' + w w' \theta' - \frac{w^2}{\eta + \kappa} \theta' \right] \\ &+ \frac{2\beta_m \lambda_m (\theta - \epsilon)}{P_r (\eta + b)^3} \left[\frac{\kappa w}{\eta + \kappa} \left\{ 1 - \frac{2}{(\eta + b)^2} \right\} - \frac{w'}{\eta + b} \right] = 0, \end{aligned} \tag{17}$$

$$\frac{1}{S_c} \left(\frac{C_1'}{\eta + \kappa} + C_1'' \right) + \frac{\delta Nt}{S_c Nb} \left(\theta'' + \frac{1}{\eta + \kappa} \theta' \right) + \frac{\kappa}{\eta + \kappa} w C_1' - \frac{\eta}{2} \delta^* C_1' - k_1 C_1 C_2^2 = 0, \tag{18}$$

$$\frac{1}{S_c} \left(\frac{C_2'}{\eta + \kappa} + C_2'' \right) + \frac{\delta Nt}{S_c Nb} \left(\theta'' + \frac{1}{\eta + \kappa} \theta' \right) + \frac{\kappa}{\eta + \kappa} w C_2' - \frac{\eta}{2} \delta^* C_2' - k_1 C_1 C_2^2 = 0, \tag{19}$$

with BCs as:

$$w' = 1 + L_1 \left(w'' - \frac{1}{k} w' \right), Me \theta' + P_r f = 0, \theta = 1, C_1' = k_2 C_1, \delta C_2' = -k_2 C_2 \text{ at } \eta = 0, w' \rightarrow 0, \quad w'' \rightarrow 0, \theta \rightarrow 0, C_1 \rightarrow 1 \text{ as } \eta \rightarrow \infty, \tag{20}$$

When pressure $P(\eta)$ is removed from Eqs. (15) and (16), we obtain:

$$\begin{aligned} \left(1 + \frac{1}{\beta}\right) \left[w'''' + \frac{2w'''}{(\eta + \kappa)^2} - \frac{w'}{(\eta + \kappa)^3} \right] \\ + We \left[(w'' w'''' + w''') - \frac{1}{(\eta + \kappa)} (w' w'''' - 2w'' w''') - \frac{2}{(\eta + \kappa)^2} (w''^2 + w' w''') + \frac{4w' w''}{(\eta + \kappa)^3} + \frac{2w'^2}{(\eta + \kappa)^4} \right] \\ + \frac{\kappa}{\eta + \kappa} [w w'''' - w' w'''] + \frac{\kappa}{(\eta + \kappa)^2} [w w'' - w'^2] - \frac{\kappa}{(\eta + \kappa)^3} w w' - \delta^* \left[\frac{\eta}{2} w'' + \frac{3w'''}{2} \right] - \frac{\delta^*}{\eta + \kappa} \left[w' + \frac{\eta}{2} w'' \right] \\ - \frac{2\beta_m}{(n + b)^4} \left[\left(\frac{1}{\eta + \kappa} - \frac{4}{\eta + b} \right) \theta + \theta' \right] + \lambda_T \left[\frac{\theta}{\eta + \kappa} + \theta' \right] - M^* \left[w'' + \frac{w'}{\eta + \kappa} \right] = 0, \end{aligned} \tag{21}$$

When $D_{C_a} = D_{C_b}, \delta = 1$ and $C_1(\eta) + C_2(\eta) = 1$ are both true. Now Eqs. (18) and (19) become:

$$\frac{1}{S_c} \left(\frac{C_1'}{\eta + \kappa} + C_1'' \right) + \frac{\kappa}{\eta + \kappa} w C_1' - k_1 C_1 (1 - C_1)^2 - \eta \delta^* C_1' = 0 \tag{22}$$

with boundary conditions:

$$C_1'(0) = k_1 C_1(0), C_1(\infty) \rightarrow 1. \tag{23}$$

Table 1 display the notations and parameters in the governing equation.

2.5. Quantities of Interest

The drag coefficient (C_{W_s}) and heat transfer rate (Na_{1s}) is defined as [15-16]:



Table 1. Notations and parameters in the governing equation.

S/N	Notations	Parameters
1	$We = \sqrt{\frac{2a^3}{a_2(1-\alpha^*t)^3}} \Gamma s$	Local Weiss Enberg number
2	$\delta^* = \frac{a^*}{a}$	Unsteadiness parameter
3	$\beta_m = \frac{\gamma\mu_0 K_1(T_w - T_\infty)\rho}{2\pi\mu^2}$	Ferro hydrodynamic interaction
4	$b = \sqrt{\frac{a}{a_2(1-\alpha^*t)}} d$	Dimensionless distance
5	$\lambda_T = \frac{Gr}{Re^2}$	Thermal Buoyancy parameter
6	$Gr = \frac{g\beta_T T_\infty(\theta_w - 1)s^3}{a_2^2}$	Corresponds to the local Grashof number
7	$M^* = \frac{\sigma\beta_0^2}{\rho a}$	Magnetic Parameter
8	$Pr = \frac{\nu}{\alpha}$	Prandtl number
9	$Rd = \frac{16\sigma^* T_\infty^3}{3kk^*}$	Radiation Parameter
10	$Nt = \frac{\tau D_T(T_w - T_\infty)}{a_2 T_\infty}$	Thermophoresis parameter
11	$Nb = \frac{\tau D_{C_b} C_0}{a_2}$	Brownian motion Parameter
12	$Ec = \frac{a_{1w}^2}{c_p(T_w - T_\infty)}$	Eckert number
13	$C_H = \lambda_1 a_1$	Thermal Relaxation Parameter
14	$\lambda_m = \frac{a\mu^2}{\rho\kappa(T_w - T_\infty)(1-\alpha^*t)}$	Heat dissipation parameter
15	$\epsilon = \frac{T_\infty}{(T_w - T_\infty)}$	Curie Temperature
16	$Q = \frac{Q_0(1-\alpha^*t)}{a(\rho c_p)}$	Heat source/ sink parameter
17	$Sc = \frac{\nu}{D_{C_a}}$	Schmidt number
18	$\delta = \frac{D_{C_b}}{D_{C_a}}$	Ratio of diffusion coefficients
19	$k_1 = \frac{C_0^2 k_c(1-\alpha^*t)}{a}$	Homogenic reaction parameter
20	$k_2 = \frac{K_1}{D_{C_a}} \sqrt{\frac{a_2(1-\alpha^*t)}{a}}$	Heterogenic reaction parameter
21	$L_1 = L_s \sqrt{\frac{a}{a_2(1-\alpha^*t)}}$	Slip parameter
22	$Me = \frac{c_p(T_w - T_\infty)}{\lambda_1 + (T_w - T_\infty)c_s}$	Melting Heat parameter
23	$Re = \frac{as^2}{a_2}$	Local Reynolds number

$$Cw_s = \frac{\tau_w}{\rho a_{1w}^2}, \text{ and } Na_{1s} = \frac{sq_w}{(T_w - T_\infty)k} \tag{24}$$

As defined by the equations below, q_w wall heat flux and τ_w wall shear stress:

$$\tau_w = \mu \left[\left(1 + \frac{1}{\beta}\right) \left(\frac{\partial a_1}{\partial r} + \frac{R}{r+R} \frac{\partial a_2}{\partial s} - \frac{a_1}{r+R}\right) + \frac{\Gamma^2}{2} \left(\frac{\partial a_1}{\partial r} + \frac{R}{r+R} \frac{\partial a_2}{\partial s} - \frac{a_1}{r+R}\right)^2 \right] \Bigg|_{r=0}, \tag{25}$$

and

$$q_w = -k \left(\frac{\partial T}{\partial r}\right) \Bigg|_{r=0} + q_r|_{r=0}, \tag{26}$$

By considering Eq. (14), the following dimensionless transformations are applied to obtain:

$$Cw_s(Re)^{\frac{1}{2}} = \left(1 + \frac{1}{\beta}\right) \left[w''(0) - \frac{1}{k}w'(0)\right] + \frac{We}{2} \left[w''(0) - \frac{1}{k}w'(0)\right]^2, \tag{27}$$

$$Na_{1s}(Re)^{\frac{1}{2}} = -[1 + Rd]\theta'(0),$$



3. Applications of Galerkin-Weighted Residual Method

In this section, the methodology and implementation of the well-known Galerkin method are discussed. The basic solution procedures of different Galerkin schemes are clarified in [58]. The major steps of the Galerkin approach are stated below:

Step 1: The first step involves examining Eqs. (21) and (22):

$$\begin{aligned} & \left(1 + \frac{1}{\beta}\right) \left[\tilde{w}'''' + \frac{2\tilde{w}'''}{(\eta + \kappa)^2} - \frac{\tilde{w}'}{(\eta + \kappa)^3} \right] \\ & + We \left[(\tilde{w}''\tilde{w}'''' + \tilde{w}''') - \frac{1}{(\eta + \kappa)} (\tilde{w}'\tilde{w}'''' - 2\tilde{w}''\tilde{w}''') - \frac{2}{(\eta + \kappa)^2} (\tilde{w}''^2 + \tilde{w}'\tilde{w}''') + \frac{4\tilde{w}'\tilde{w}''}{(\eta + \kappa)^3} + \frac{2\tilde{w}'^2}{(\eta + \kappa)^4} \right] \\ & + \frac{\kappa}{\eta + \kappa} [\tilde{w}\tilde{w}'''' - \tilde{w}'\tilde{w}'''] + \frac{\kappa}{(\eta + \kappa)^2} [\tilde{w}\tilde{w}'' - \tilde{w}'^2] - \frac{\kappa}{(\eta + \kappa)^3} \tilde{w}\tilde{w}' - \delta^* \left[\frac{\eta}{2} \tilde{w}'' + \frac{3\tilde{w}'''}{2} \right] - \frac{\delta^*}{\eta + \kappa} \left[\tilde{w}' + \frac{\eta}{2} \tilde{w}'' \right] \\ & - \frac{2\beta_m}{(n + b)^4} \left[\left(\frac{1}{\eta + \kappa} - \frac{4}{\eta + b} \right) \tilde{\theta} + \tilde{\theta}' \right] + \lambda_T \left[\frac{\tilde{\theta}}{\eta + \kappa} + \tilde{\theta}' \right] - M^* \left[\tilde{w}'' + \frac{w'}{\eta + \kappa} \right] = 0, \end{aligned} \quad (28)$$

$$\begin{aligned} & \frac{1}{Pr} [1 + Rd] \left(\frac{1}{(\eta + \kappa)} \tilde{\theta}' + \tilde{\theta}'' \right) + \frac{\kappa}{\eta + \kappa} \tilde{w}\tilde{\theta}' + NbC_1'\tilde{\theta}' + Nt\tilde{\theta}'' - \frac{\eta}{2} \delta^* \tilde{\theta}' + EcM^*\tilde{w}'^2 + Q\tilde{\theta}e^{-n} - C_H \left(\frac{\kappa}{\eta + \kappa} \right)^2 \left[\tilde{w}^2\tilde{\theta}' + \tilde{w}\tilde{w}'\tilde{\theta}' - \frac{\tilde{w}^2}{\eta + \kappa} \tilde{\theta}' \right] \\ & + \frac{2}{Pr} \frac{\beta_m \lambda_m (\tilde{\theta} - \epsilon)}{(\eta + b)^3} \left[\frac{\kappa w}{\eta + \kappa} \left\{ 1 - \frac{2}{(\eta + b)^2} \right\} - \frac{\tilde{w}'}{\eta + b} \right] = 0, \end{aligned} \quad (29)$$

$$\frac{1}{S_c} \left(\frac{C_1'}{\eta + \kappa} + C_1'' \right) + \frac{\kappa}{\eta + \kappa} wC_1' - k_1 C_1 (1 - C_1)^2 - \eta \delta^* C_1' = 0, \quad (30)$$

Step 2: The Galerkin method in Step two utilizes a specific trial function to simulate the numerical results of formula (28) to (30), which can be examined as follows.

$$\tilde{w}(\eta) = m^*_0 + m^*_1 e^{-\frac{\eta}{3}} + m^*_2 e^{-\frac{2\eta}{3}} + m^*_3 e^{-2\eta} + \dots + m^*_n e^{-\frac{n\eta}{3}} = \sum_{j=0}^n m^*_j e^{-\frac{j\eta}{3}}, \quad (31)$$

$$\tilde{\theta}(\eta) = h^*_0 + h^*_1 e^{-\frac{\eta}{3}} + h^*_2 e^{-\frac{2\eta}{3}} + h^*_3 e^{-2\eta} \dots + h^*_n e^{-\frac{n\eta}{3}} = \sum_{j=0}^n h^*_j e^{-\frac{j\eta}{3}}, \quad (32)$$

$$\tilde{C}_1(\eta) = p^*_0 + p^*_1 e^{-\frac{\eta}{3}} + p^*_2 e^{-\frac{2\eta}{3}} + p^*_3 e^{-2\eta} \dots + p^*_n e^{-\frac{n\eta}{3}} = \sum_{j=0}^n p^*_j e^{-\frac{j\eta}{3}}, \quad (33)$$

Step 3: In the second step, the trial solutions obtained using the GWRM must adhere to the specified BCs for Eqs. (21) and (22). By employing the BCs provided in Eq. (20), the following trial solutions were derived:

$$\begin{aligned} & \left(\frac{d}{d\eta} \sum_{j=0}^n m^*_j e^{-\frac{j\eta}{3}} - L_1 \left(\frac{d^2}{d\eta^2} \sum_{j=0}^n m^*_j e^{-\frac{j\eta}{3}} - \frac{1}{K} \frac{d}{d\eta} \sum_{j=0}^n m^*_j e^{-\frac{j\eta}{3}} \right) \right)_{\eta=0} = 0, \quad \left(Me \frac{d}{d\eta} \sum_{j=0}^n h^*_j e^{-\frac{j\eta}{3}} + Pr \sum_{j=0}^n m^*_j e^{-\frac{j\eta}{3}} \right)_{\eta=0} = 0, \\ & \left(\sum_{j=0}^n h^*_j e^{-\frac{j\eta}{3}} - 1 \right)_{\eta=0} = 0, \\ & \left(\frac{d}{d\eta} \sum_{j=0}^n p^*_j e^{-\frac{j\eta}{3}} - K_1 \sum_{j=0}^n p^*_j e^{-\frac{j\eta}{3}} \right)_{\eta=0} = 0. \end{aligned} \quad (34)$$

Step 4: Residual vectors for $\tilde{w}(\eta)$, $\tilde{\theta}(\eta)$, and $\tilde{C}_1(\eta)$ are produced in the fourth step via applying the reduced trial solutions to the technique outlined in step one:

$$\begin{aligned} R_w &= \left(1 + \frac{1}{\beta}\right) \left[\tilde{w}'''' + \frac{2\tilde{w}'''}{(\eta + \kappa)^2} - \frac{\tilde{w}'}{(\eta + \kappa)^3} \right] \\ & + We \left[(\tilde{w}''\tilde{w}'''' + \tilde{w}''') - \frac{1}{(\eta + \kappa)} (\tilde{w}'\tilde{w}'''' - 2\tilde{w}''\tilde{w}''') - \frac{2}{(\eta + \kappa)^2} (\tilde{w}''^2 + \tilde{w}'\tilde{w}''') + \frac{4\tilde{w}'\tilde{w}''}{(\eta + \kappa)^3} + \frac{2\tilde{w}'^2}{(\eta + \kappa)^4} \right] \\ & + \frac{\kappa}{\eta + \kappa} [\tilde{w}\tilde{w}'''' - \tilde{w}'\tilde{w}'''] + \frac{\kappa}{(\eta + \kappa)^2} [\tilde{w}\tilde{w}'' - \tilde{w}'^2] - \frac{\kappa}{(\eta + \kappa)^3} \tilde{w}\tilde{w}' - \delta^* \left[\frac{\eta}{2} \tilde{w}'' + \frac{3\tilde{w}'''}{2} \right] - \frac{\delta^*}{\eta + \kappa} \left[\tilde{w}' + \frac{\eta}{2} \tilde{w}'' \right] \\ & - \frac{2\beta_m}{(n + b)^4} \left[\left(\frac{1}{\eta + \kappa} - \frac{4}{\eta + b} \right) \tilde{\theta} + \tilde{\theta}' \right] + \lambda_T \left[\frac{\tilde{\theta}}{\eta + \kappa} + \tilde{\theta}' \right] - M^* \left[\tilde{w}'' + \frac{w'}{\eta + \kappa} \right] \cong 0, \end{aligned} \quad (35)$$

$$\begin{aligned} R_\theta &= \frac{1}{Pr} [1 + Rd] \left(\frac{1}{(\eta + \kappa)} \tilde{\theta}' + \tilde{\theta}'' \right) + \frac{\kappa}{\eta + \kappa} \tilde{w}\tilde{\theta}' + NbC_1'\tilde{\theta}' + Nt\tilde{\theta}'' - \frac{\eta}{2} \delta^* \tilde{\theta}' + EcM^*\tilde{w}'^2 + Q\tilde{\theta}e^{-n} \\ & - C_H \left(\frac{\kappa}{\eta + \kappa} \right)^2 \left[\tilde{w}^2\tilde{\theta}' + \tilde{w}\tilde{w}'\tilde{\theta}' - \frac{\tilde{w}^2}{\eta + \kappa} \tilde{\theta}' \right] + \frac{2}{Pr} \frac{\beta_m \lambda_m (\tilde{\theta} - \epsilon)}{(\eta + b)^3} \left[\frac{\kappa w}{\eta + \kappa} \left\{ 1 - \frac{2}{(\eta + b)^2} \right\} - \frac{\tilde{w}'}{\eta + b} \right] \cong 0, \end{aligned} \quad (36)$$

$$R_{C_1} = \frac{1}{S_c} \left(\frac{C_1'}{\eta + \kappa} + C_1'' \right) + \frac{\kappa}{\eta + \kappa} wC_1' - k_1 C_1 (1 - C_1)^2 - \eta \delta^* C_1' \cong 0, \quad (37)$$



Table 2. Comparison of Nusselt number for different values of Prandtl number.

k	5	10	20	30	40	50
Result of [18]	1.15763	1.07349	1.03561	1.02353	1.01759	1.01405
Result of [45]	1.15763	1.07349	1.03561	1.02353	1.01759	1.01405
Current result	1.15763	1.07349	1.03561	1.02353	1.01759	1.01405

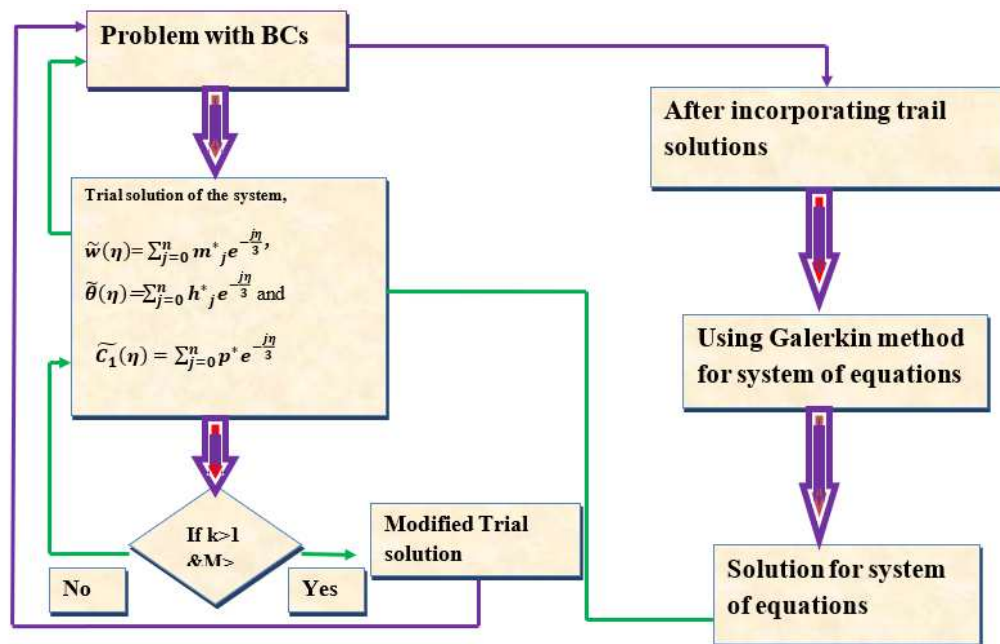


Fig. 3. The Galerkin Weighted Residual method flow chart.

Step 5: Now, to examine the constants, the residual must be zero over the discussed domain as given below:

$$\begin{aligned}
 \int_0^\infty R_w e^{-\frac{j\eta}{3}} d\eta &\approx \sum_{k=1}^j [A_k (e^\eta R_w e^{-\frac{j\eta}{3}})_{\eta=x_k}] = 0, \\
 \int_0^\infty R_\theta e^{-\frac{j\eta}{3}} d\eta &\approx \sum_{k=1}^j [A_k (e^\eta R_\theta e^{-\frac{j\eta}{3}})_{\eta=x_k}] = 0, \\
 \int_0^\infty R_{C_1} e^{-\frac{j\eta}{3}} d\eta &\approx \sum_{k=1}^j [A_k (e^\eta R_{C_1} e^{-\frac{j\eta}{3}})_{\eta=x_k}] = 0,
 \end{aligned}
 \tag{38}$$

For $j = 0, 1, 2, \dots, N - 2, l = 0, 1, 2, \dots, N - 2$ to zero.

where A_k is described as:

$$A_k = \frac{1}{L'_j(x_k)} \int_0^\infty \frac{L_j(x) e^{-x}}{x - x_k} dx = \frac{(j!)^2}{x_k (L'_j(x_k))^2}, L_j = e^x \frac{d^j}{dx^j} (e^{-x} x^j)
 \tag{39}$$

The unknown coefficients were computed using a mathematical tool by minimizing the weight functions $R_w e^{-\frac{j\eta}{3}}$, $R_\theta e^{-\frac{j\eta}{3}}$ and $R_{C_1} e^{-\frac{j\eta}{3}}$ associated with the residual errors. The agreement between the Current result and previously published result, as displayed in Table 2, confirms the validation of the current solutions. The comparison clearly reveals a high level of agreement between the results. The flow chart of the GWRM scheme is shown in Table 2. Figure 3 displays the Galerkin weighted residual method flow chart.

4. Results and Discussion

The influence of different control parameters on fluid flow, thermal profile, and concentration profile, denoted as $w'(\eta)$, $\theta(\eta)$ and $C_1(\eta)$, respectively, is visually represented in this section using graphical illustrations. Unless explicitly specified in the graphs or tables, the parameters involved in this problem have been assigned numerical values as: $\lambda_T = \beta_m = L_1 = 0.4$, $\delta^* = Q = 0.1$, $Rd = \lambda_m = \epsilon = 0.2$, $C_H = 0.2$, $k_2 = k_1 = 0.5$, $M^* = 2$.

4.1. Effects of magnetic parameter M^* and dimensionless distance parameter b on fluid flow $w'(\eta)$

The magnetic field is a non-dimensional value that describes the ratio between the strength of the magnetic field and the viscous forces exerted on an electrically conducting liquid. This magnetic field assists to calculate the relative effect of these two features. The $w'(\eta)$ of an electrically conducting liquid is significantly induced via the M . When a liquid is exposed to a magnetic field, it experiences a Lorentz force. The $w'(\eta)$ of a Casson-Williamson NFs over a stretching surface is induced via the M , as illustrated in Fig. 4. This figure shows the $w'(\eta)$ associated with changing values of the M . The reduction in $w'(\eta)$ is revealed via a



lower $w'(\eta)$ as the M improves. This indicates that as the M rises, the $w'(\eta)$ reduces. The $w'(\eta)$ near the momentum boundary layer is elevated, lead to the intense drag force when a surface is stretched. This drags force, which opposes the $w'(\eta)$, causes a reduction in the fluid flow close the boundary layer. Also, the $w'(\eta)$ is greater near the momentum boundary layer, resulting in the intense magnetic field. Therefore, the Lorentz force is also effective near the momentum boundary layer, causing a more substantial reduction in $w'(\eta)$. Physically, in magnetohydrodynamic (MHD) generators, the M is employed to regulate the $w'(\eta)$ of a fluid. This is attained via employing a magnetic field perpendicular to the flow of an electrically conducting liquid. The Lorentz force operates on the liquid, causing it to slow down and convert its kinetic energy into electrical energy. Furthermore, the dimensional distance parameter illustrates how quickly a surface is stretched. The $w'(\eta)$ of a NFs over a stretching surface is described in Fig. 5, showing the influence of the b parameter. The increase in the b leads to a lower $w'(\eta)$, which shows an improvement in the fluid flow. Physically, the design of heat exchangers is realistic operation where the b parameter is utilized in NFs boundary layer flows. To boost the thermal transport rate in heat exchangers, increasing the surface area is essential. This can be achieved via featuring a stretching surface, which enables the transport of heat from one fluid to another.

4.2. Influence of ferrohydrodynamic interaction β_m and thermal buoyancy parameter λ_T on fluid flow $w'(\eta)$

The β_m quantifies the magnetic interaction between ferromagnetic nanoparticles (NPs) and the base liquid in a NFs. The β_m signifies the relative intensity of this interaction. The $w'(\eta)$ of a stretching surface of the NFs boundary layer flow is significantly influenced via the β_m as observed in Fig. 6. The ferromagnetic NPs in a nanofluid arises when a magnetic field is applied, resulting in the production of a magnetic dipole moment in each NPs. The magnetic field applied perpendicular to the movement of the NFs in boundary layer (BL) flow over a stretching surface result in the ferrohydrodynamic force performing in the same direction as the magnetic field. The ferrohydrodynamic force be in opposition to the movement of the NFs, resulting in a slowing down the $w'(\eta)$ as it behaves in the opposite path of the flow movement. A realistic application of the ferrohydrodynamic interaction parameter in nanofluid BL flows can be observed in the improvement of drug delivery systems. These systems are operated to deliver drugs to the body systems in accurate way. One useful method to achieve controlled drug delivery is by using NFs. The $w'(\eta)$ of the NFs in a drug delivery system can be improved by strengthening the β_m .

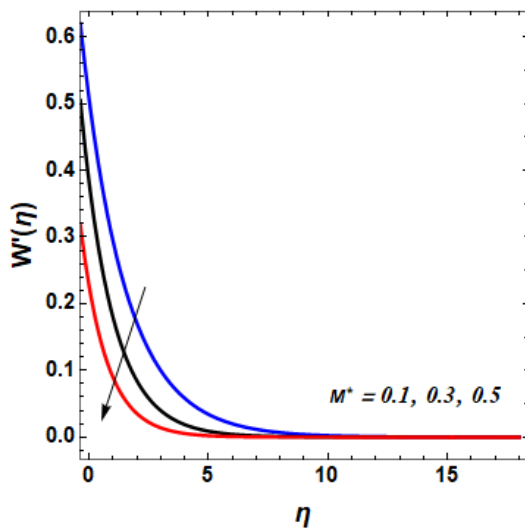


Fig. 4. Effect of M^* on $w'(\eta)$.

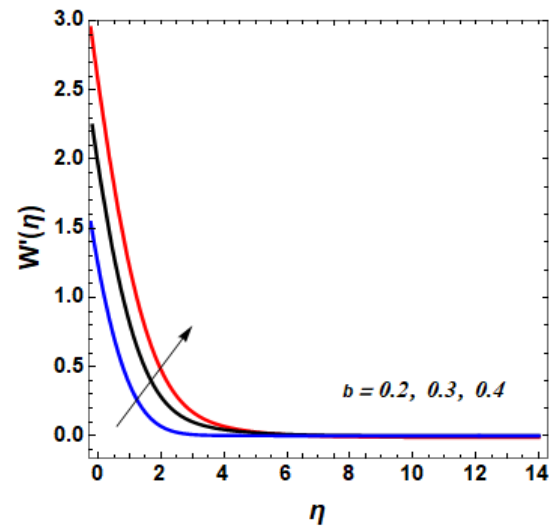


Fig. 5. Effect of b on $w'(\eta)$.

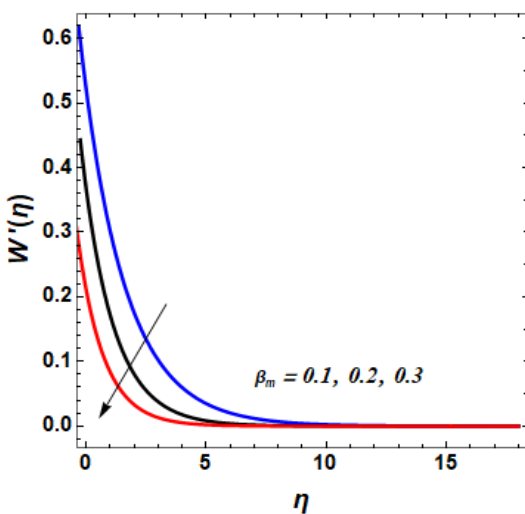


Fig. 6. Impact of β_m on $w'(\eta)$.

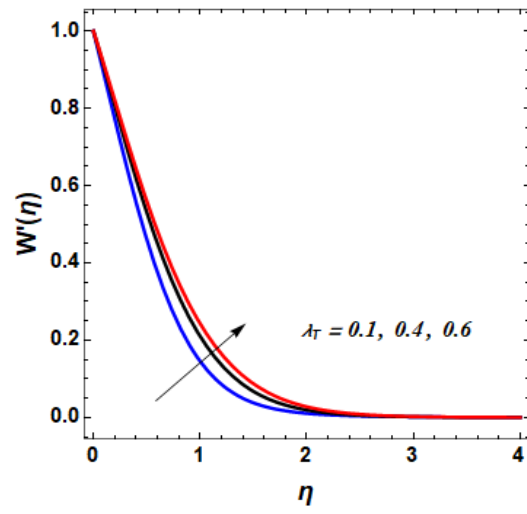


Fig. 7. Impact of λ_T on $w'(\eta)$.



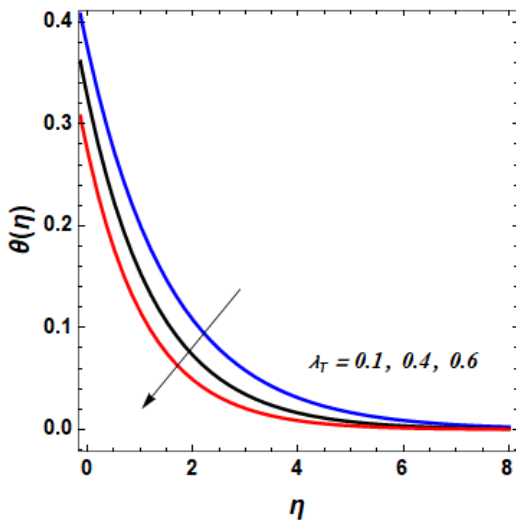


Fig. 8. Impact of λ_T on $\theta(\eta)$.

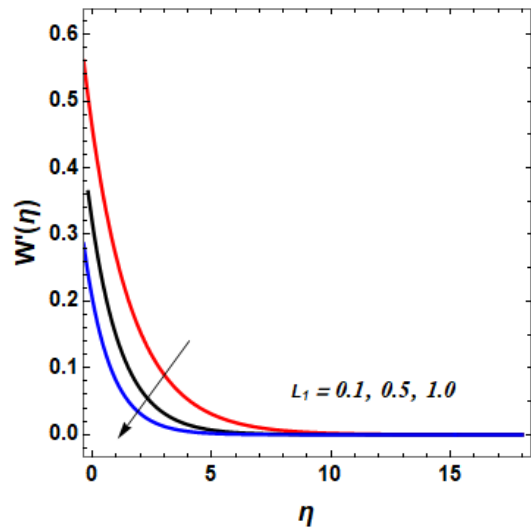


Fig. 9. Impact of L_1 on $w'(\eta)$.

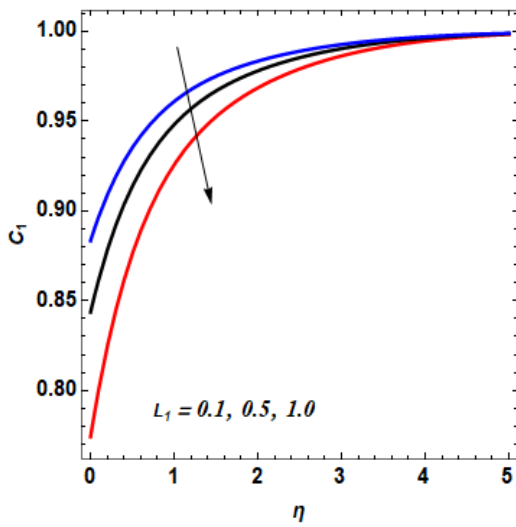


Fig. 10. Influence of L_1 on $C_1(\eta)$.

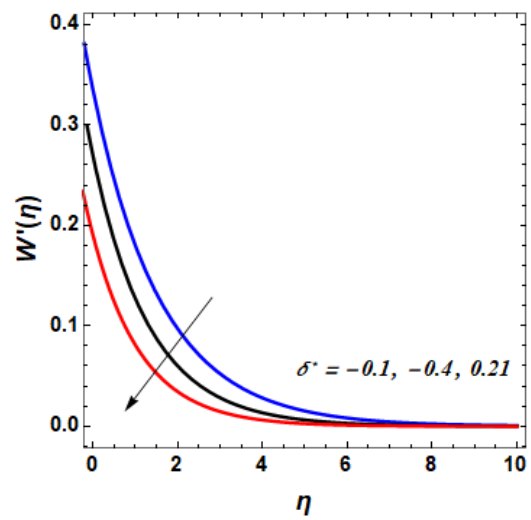


Fig. 11. Impact of δ^* on $w'(\eta)$.

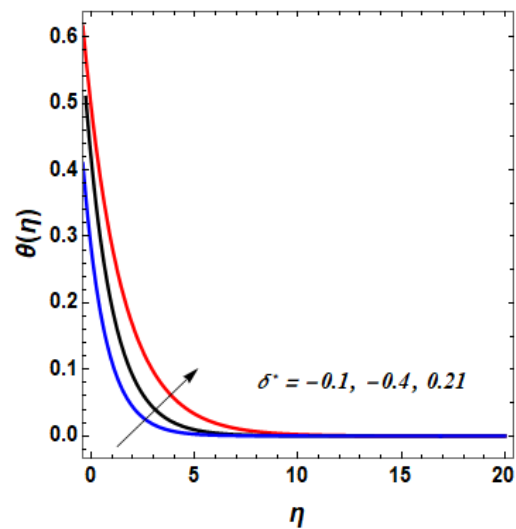


Fig. 12. Impact of δ^* on $\theta(\eta)$.

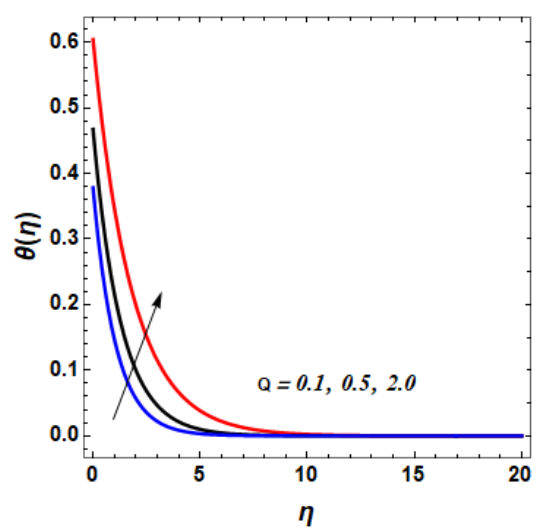


Fig. 13. Impact of Q on $\theta(\eta)$.



This advancement supports quicker and more effective delivery of the drug to the intended position within the body systems. The λ_T characterizes the ratio of the buoyancy force to the viscous forces in a fluid. The $w'(\eta)$ greatly inspired by the λ_T as it was observed in Fig. 7. The heating of a liquid results in its enlargement, leading to a decrease in liquid density. The decrease in density leads to the expansion of the liquid, generating a buoyancy force that opposes gravity and tends to elevate the vertical velocity component $w'(\eta)$. Additionally, Fig. 8. shows an increase in the effect of λ_T . Therefore, the parameter λ_T is observed in the development of solar thermal collectors within the context of boundary layer flows. These collectors are operated to gather heat from the sun and transfer it to a working fluid. Therefore, by employing a NFs is an active procedure to boost the thermal transport rate in a solar thermal collector.

4.3. Influence of slip parameter L_1 and unsteadiness parameter δ^* on fluid flow $w'(\eta)$ and fluid temperature $\theta(\eta)$

The L_1 quantifies the ratio between the slip velocity and the no-slip boundary condition. The speed of the liquid at the surface exceeds the velocity of the wall when slip arises. The motive for this is that the molecules of the liquid at the interface are not adhered to the surface and have the capacity to transfer without restriction. The $w'(\eta)$ and $C_1(\eta)$ reduced close the surface, while it is intensified distant away from the surface.

Figures 9 and 10 clearly illustrate the influence of the velocity slip factor's de-escalation on the velocity distribution. In stretched sheets and fluid flows, an increase in velocity slip creates heterogenic velocity, which results in a decrease in the velocity distribution. Physically, Slip is utilized in microfluidic machines to control liquid movement at the microscale. An example of its application is seen in the reduction of pressure drop within microfluidic channels, thereby enhancing the performance of such devices. Moreover, slip is utilized in thermal transport to augment the rate of heat transfer. For instance, slip can be employed to alleviate thermal resistance in heat exchangers, ultimately improving the efficiency of the heat transfer process. The δ^* quantifies the implication of unsteady influences within a $w'(\eta)$ supplying helpful understanding into the dynamics of the fluid system. The $w'(\eta)$ is influenced via the δ^* . In a steady flow, the $w'(\eta)$ remains constant over time at each point in the flow. On the other hand, in an unsteady flow, the $w'(\eta)$ at each point in the flow changes with time. From Figs. 11 and 12, it was observed that the δ^* elevate the $w'(\eta)$. Physically, the movement of fluids in numerous purposes can be controlled using the δ^* . This δ^* has the capacity to slow down the drag on motor vehicle and airplanes, as well as boost the productivity of heat exchangers. The δ^* can be utilized to boost the combining of liquids. This can be suitable in applications including drug delivery and chemical industry operations.

4.4. Impact of Heating generation Q and Melting parameter Me on fluid temperature $\theta(\eta)$

Heat generation parameter refers to a factor that represents the rate at which heat is generated within a fluid. In various physical systems, heat generation can occur due to different mechanisms, such as chemical reactions, electrical currents, or other sources. The heat generation parameter quantifies the intensity of heat produced per unit volume or unit mass within the fluid. The increased heat generation parameter causes an overall elevation of the fluid temperature (see Fig. 13). The $\theta(\eta)$ of the fluid reduces as the Me increases (see Fig. 14). The temperature of the liquid slow down as the solid needs more energy to melt due to a higher melting heat parameter. Physically, the release of the latent heat of fusion of water when food is frozen causes a reduce in the temperature of the freezer. This experience occurs as the freezer absorbs the heat released through the freezing process.

4.5. Impacts of thermal radiation Rd and heat dissipation parameter λ_m fluid temperature $\theta(\eta)$

Thermal radiation (Rd) plays a key role in the design of different practical usages, such as cooling and manufacturing, solar panels and collectors, nuclear reactors, generating electricity. The thermal radiation, together with conduction and convection, are important techniques of transmitting thermal energy. It encompasses the transport of heat via electromagnetic waves. The significance of Rd and conduction thermal transport in a fluid system can be established by exploring the thermal radiation parameter. A small value of Rd shows that conduction thermal transport is dominant, whereas a larger value of Rd shows that thermal radiation is dominant. Rd is more effective in transporting heat over long distances compared to conduction thermal transport. This effect is observed in Fig. 15. The λ_m quantifies the effectiveness of a system in releasing heat to its environment. From Fig. 16, it was seen that the λ_m reduce the fluid temperature. Physically, high λ_m indicates efficient heat dissipation to the surrounding fluid, resulting in quicker thermal transport and a more uniform temperature distribution. On other hand, if the λ_m is reduced, the fluid system's power to dissipate heat is reduced, resulting in slow-moving thermal transport. The Curie temperature (ϵ) is a characteristic of ferromagnetic and some other materials that relates to their properties.

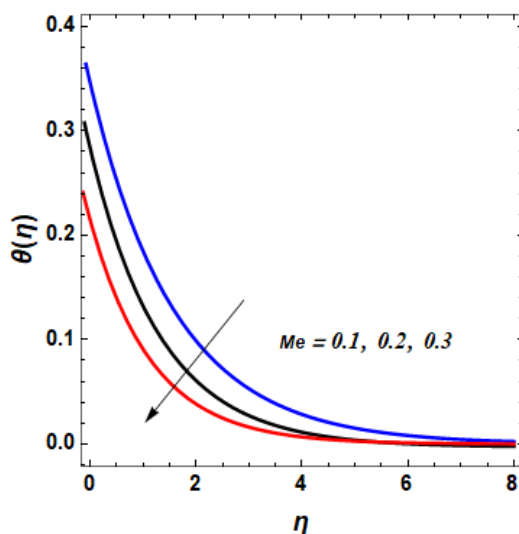


Fig. 14. Impact of Me on $\theta(\eta)$.

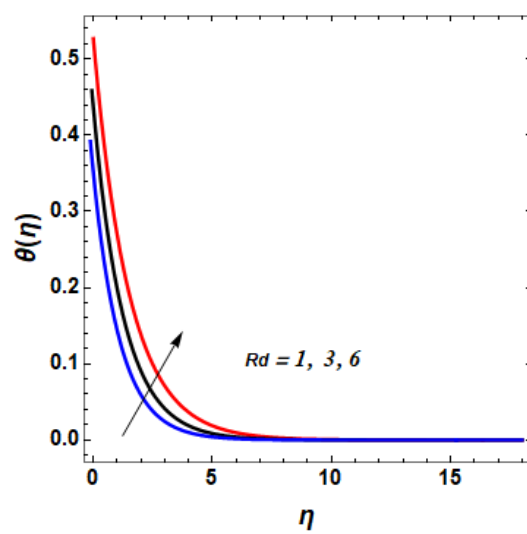


Fig. 15. Impact of Rd on $\theta(\eta)$.



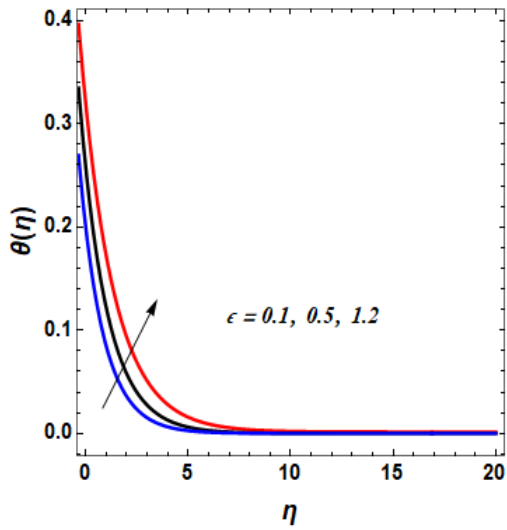


Fig. 16. Impact of ϵ on $\theta(\eta)$.

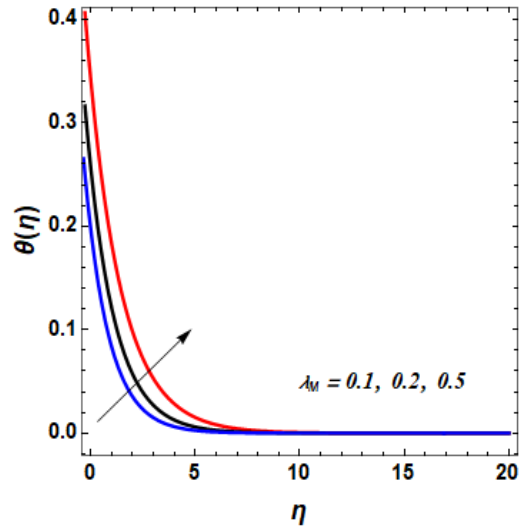


Fig. 17. Influence of λ_m on $\theta(\eta)$.

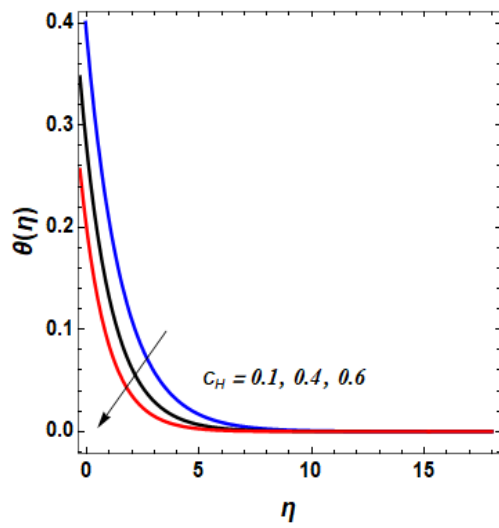


Fig. 18. Impact of C_H on $\theta(\eta)$.

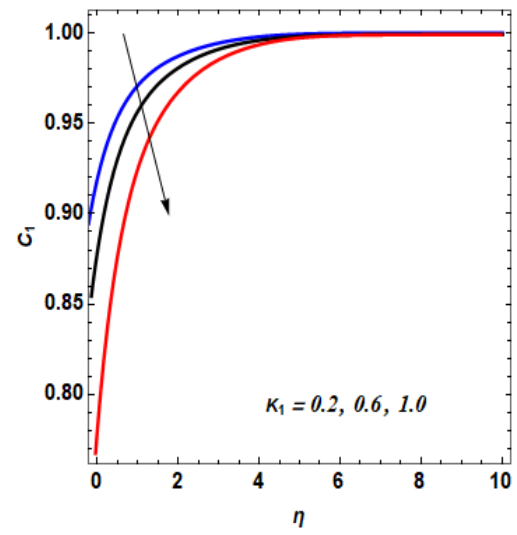


Fig. 19. Impact of k_1 on C_1 .

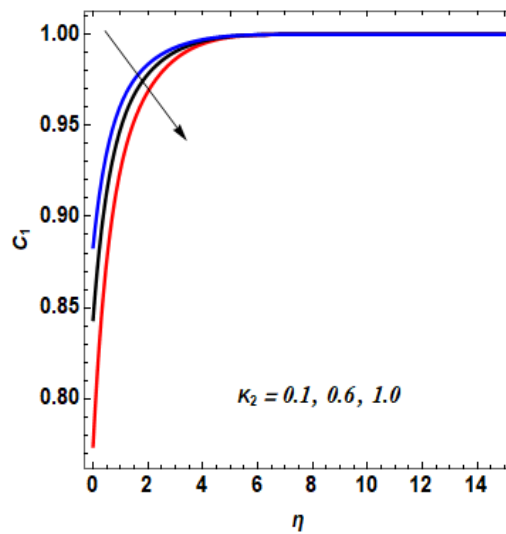


Fig. 20. Influence of k_2 on C_1 .



From Fig. 17, it was observed that the $\theta(\eta)$ reduced by the ϵ parameter. Additionally, the Cattaneo-Christov parameter, which is usually denoted to as the thermal relaxation parameter, is a non-dimensional value that defines the duration needed for a liquid to attain thermal balance with its environment. Figure 18 demonstrates the variations in temperature regime with rising Curie temperature values. The decline in heat flux happens due to the C_H influence on the transport of thermal process. This C_H slow down the temperature gradient near a heated surface, thereby declining the driving force for heat conduction. Physically, the decrease in the $\theta(\eta)$ is attributed to the C_H , which considers the internal energy of the fluid system. The internal energy of a fluid implies to the energy correlated to the movement of its particles. When heating a fluid, its internal energy improves, leading to enlargement and a subsequent reduction in the temperature gradient near a heated surface.

4.6. Impacts of homogeneous reaction parameter k_1 and homogenic reaction parameter k_2 on the concentration profile C_1

A homogeneous reaction refers to a chemical reaction in which all reacting species are present in the same phase, typically as gases or dissolved in a liquid. In contrast, a heterogeneous reaction involves species in different phases, such as a gas reacting with a solid. The presence of homogeneous reactions can lead to a reduction in the concentration profile due to the consumption of reactants and the production of products within the reaction medium. (see Fig. 19). The k_2 the ratio of the rate of heterogeneous reactions to the diffusion rate and quantifies the relative quantity of reactions at the surface compared to bulk fluid. A greater k_2 value signifies a superior impact of heterogeneous reactions, while a lower value implies a more significant role of diffusion processes. The parameter C_1 is greatly affected by the heterogenic parameter. As the value of C_1 rises, the reactant concentration at the surface decreases, resulting in a reducing concentration gradient (see Fig. 20).

5. Conclusions

In conclusion, this study investigated the Ferrohydrodynamic interaction analysis of unsteady nanofluid flow over a curved stretching sheet with melting heat peripheral conditions. Also, the mathematical model considers various factors, including the effects of Cattaneo-Christov heat flux, buoyancy effect, thermal radiation, nanofluid and exponential heat source. The Galerkin-weighted residual technique was employed to numerically solve the governing equations after they were transformed into a non-dimensional form. Below are the notable factors examined during the parametric studies, which were investigated using figures and tables to visually represent the findings.

- The thermal buoyancy parameter reduces the $w'(\eta)$ and $\theta(\eta)$.
- Both the heterogenic reaction parameter and the homogenic reaction parameter reduce the $C_1(\eta)$.
- The heat source/sink parameter, radiation parameter, and Curie temperature have a significant impact on the $\theta(\eta)$.
- An increase in the curie temperature leads to a rise in the $w'(\eta)$. Similarly, other parameters, including the ferrohydrodynamic interaction, slip parameter, and Magnetic field parameter display a consistent trend of reducing the $w'(\eta)$.
- The fluid temperature is significantly enhanced by the unsteadiness parameter, while the thermal relaxation parameter, heat dissipation, thermal Buoyancy, and melting heat parameter, and temperature slip constraints collectively diminish it.

Future recommendations

In the near future, the scientists should aim to inspect how various magnetic dipole configurations and steady flow conditions influence the flow properties of nanofluids. Furthermore, it would be useful to conduct experimental studies to confirm the accuracy of the computational result. The Galerkin-weighted residual method holds the potential to address a wide range of physical and technical challenges that may arise in the future.

Author Contributions

A.M. Obalalu planned the scheme, initiated the project, and suggested the experiments; A. Darvesh & A.O. Akindele conducted the experiments and analyzed the empirical results; A. Phulpoto & A.D. Adeshola developed the mathematical modeling and examined the theory validation. The manuscript was written through the contribution of all authors. All authors discussed the results, reviewed, and approved the final version of the manuscript.

Acknowledgments

Not applicable.

Conflict of Interest

The authors declared no potential conflicts of interest concerning the research, authorship, and publication of this article.

Funding

Not applicable.

Data Availability Statements

Not applicable.

Nomenclature and Abbreviations List

k	Thermal conductivity	q_r	Radiative heat flux
D_{C_a}	Diffusion coefficient of A	H	Magnetic field



β	Casson parameter	β_T	Coefficient of thermal expansion
λ_1	Relaxation time of heat	c_s	Heat capacity of the solid surface
T_∞	Ambient fluid temperature	D_T	Thermophoretic diffusion coefficient
T	Temperature	L_s	Velocity slip coefficient
T_w	Temperature of the fluid at the surface	Q_0	Space dependent heat source
Γ	Material time constant	T_m	Melting temperature,
α	Thermal diffusivity	(a_1, a_2)	Velocities along
(s, r)	Orientations	(k_c, k_s)	Rate constant
ρ	Density	T_0	Temperature of the solid surface
k	Curvature parameter	D_{C_b}	Diffusion coefficient of b
τ	Ratio of the effective heat capacity	λ_l	Latent heat of fluid
σ	Electrical conductivity	c_p	Specific heat
ν	Kinematic viscosity	μ_0	Magnetic permeability
M	Magnetization	B_0	Constant magnetic field
g	Acceleration,	K_1	Ferromagnetic coefficient
p	Pressure	k^*	Coefficient of mean absorption
σ^*	Stefan-Boltzmann constant	γ	Intensity of the magnetic field
d	Distance between the dipole	$C_1(\eta)$	Homogeneous concentration
$w'(\eta)$	Velocity	η	Cohesive variable
$C_2(\eta)$	Heterogeneous concentration	$\theta(\eta)$	Temperature
$P(\eta)$	Pressure		

References


- [1] Wen, D., Lin, G., Vafaei, S., Zhang, K., Review of nanofluids for heat transfer applications, *Particuology*, 7(2), 2009, 141-150.
- [2] Wu, D., Zhu, H., Wang, L., Liu, L., Critical issues in nanofluids preparation, characterization, and thermal conductivity, *Current Nanoscience*, 5(1), 2009, 103-112.
- [3] Saidur, R., Leong, K.Y., Mohammed, H.A., A review on applications and challenges of nanofluids, *Renewable and Sustainable Energy Reviews*, 15(3), 2011, 1646-1668.
- [4] Bhogare, R.A., Kothawale, B.S., A review on applications and challenges of nanofluids as coolant in automobile radiator, *International Journal of Scientific and Research Publications*, 3(8), 2013, 1-11.
- [5] Sajid, M.U., Ali, H.M., Recent advances in the application of nanofluids in heat transfer devices: a critical review, *Renewable and Sustainable Energy Reviews*, 103, 2019, 556-592.
- [6] Younes, H., Mao, M., Murshed, S.S., Lou, D., Hong, H., Peterson, G.P., Nanofluids: Key parameters to enhance thermal conductivity and its applications, *Applied Thermal Engineering*, 207, 2022, 118202.
- [7] Nagaraja, K.V., et al., Thermal conductivity performance in sodium alginate based Casson nanofluid flow by a curved Riga surface, *Frontiers in Materials*, 10, 2023, 1253090.
- [8] Darvesh, A., Altamirano, G.C., Sánchez-Chero, M., Zamora, W.R., Campos, F.G., Sajid, T., Ayub, A., Variable chemical process and radiative nonlinear impact on magnetohydrodynamics Cross nanofluid: An approach toward controlling global warming, *Heat Transfer*, 52(3), 2023, 2559-2575.
- [9] Madhukesh, J.K., Sarris, I.E., Vinutha, K., Prasannakumara, B.C., Abdulrahman, A., Computational analysis of ternary nanofluid flow in a microchannel with nonuniform heat source/sink and waste discharge concentration, *Numerical Heat Transfer, Part A: Applications*, 2023, DOI: 10.1080/10407782.2023.2240509.
- [10] Madhukesh, J.K., Paramesh, S.O., Prasanna, G.D., Prasannakumara, B.C., Khan, M.I., Abdullaev, S., Rasool, G., Impact of magnetized nanoparticle aggregation over a Riga plate with thermal radiation in water-Al₂O₃ based nanofluid flow, *ZAMM-Journal of Applied Mathematics and Mechanics/Zeitschrift für Angewandte Mathematik und Mechanik*, 2024, e202300270.
- [11] Assael, M.J., Antoniadis, K.D., Wakeham, W.A., Zhang, X., Potential applications of nanofluids for heat transfer, *International Journal of Heat and Mass Transfer*, 138, 2019, 597-607.
- [12] Yousef, N.S., Megahed, A.M., Ghoneim, N.I., Elsafi, M., Fares, E., Chemical reaction impact on MHD dissipative Casson-Williamson nanofluid flow over a slippery stretching sheet through porous medium, *Alexandria Engineering Journal*, 61(12), 2022, 10161-10170.
- [13] Humane, P.P., Patil, V.S., Patil, A.B., Chemical reaction and thermal radiation effects on magnetohydrodynamics flow of Casson-Williamson nanofluid over a porous stretching surface, *Proceedings of the Institution of Mechanical Engineers, Part E: Journal of Process Mechanical Engineering*, 235(6), 2021, 2008-2018.
- [14] Mangathai, P., Unsteady MHD Williamson and Casson nano fluid flow in the presence of radiation and viscous dissipation, *Turkish Journal of Computer and Mathematics Education*, 12(13), 2021, 1036-1051.
- [15] Salawu, S.O., Obalalu, A.M., Fatunmbi, E., Oderinu, R., Thermal Prandtl-Eyring hybridized MoS₂-SiO₂/C₃H₈O₂ and SiO₂-C₃H₈O₂ nanofluids for effective solar energy absorber and entropy optimization: a solar water pump implementation, *Journal of Molecular Liquids*, 361, 2022, 119608.
- [16] Olayemi, O.A., Obalalu, A.M., Odetunde, C.B., Ajala, O.A., Heat transfer enhancement of magnetized nanofluid flow due to a stretchable rotating disk with variable thermophysical properties effects, *The European Physical Journal Plus*, 137, 2022, 1-12.
- [17] Madhukesh, J.K., Kumar, R.N., Gowda, R.P., Prasannakumara, B.C., Ramesh, G.K., Khan, M.I., Chu, Y.M., Numerical simulation of AA7072-AA7075/water-based hybrid nanofluid flow over a curved stretching sheet with Newtonian heating: A non-Fourier heat flux model approach, *Journal of Molecular Liquids*, 335, 2021, 116103.
- [18] Kumar, P., Nagaraja, B., Almeida, F., AjayKumar, A.R., Al-Mdallal, Q., Jarad, F., Magnetic dipole effects on unsteady flow of Casson-Williamson nanofluid propelled by stretching slippery curved melting sheet with buoyancy force, *Scientific Reports*, 13(1), 2023, 12770.
- [19] Falodun, B.O., Ige, E.O., Linear and quadratic multiple regressions analysis on magneto-thermal and chemical reactions on the Casson-Williamson nanofluids boundary layer flow under Soret-Dufour mechanism, *Arab Journal of Basic and Applied Sciences*, 29(1), 2022, 269-286.
- [20] Obalalu, A.M., Adebayo, L.L., Colak, I., Ajala, A.O., Wahaab, F.A., Entropy generation minimization on electromagnetohydrodynamic radiative Casson nanofluid flow over a melting Riga plate, *Heat Transfer*, 51(5), 2022, 3951-3978.
- [21] Obalalu, A., Oreyeni, T., Abbas, A., Memon, M.A., Khan, U., Sherif, E.S.M., Hassan, A.M., Pop, I., Implication of electromagnetohydrodynamic and heat transfer analysis in nanomaterial flow over a stretched surface: applications in solar energy, *Case Studies in Thermal Engineering*, 49, 2023, 103381.
- [22] Haq, I., Naveen Kumar, R., Gill, R., Madhukesh, J.K., Khan, U., Raizah, Z., Jirawattanapanit, A., Impact of homogeneous and heterogeneous reactions in the presence of hybrid nanofluid flow on various geometries, *Frontiers in Chemistry*, 10, 2022, 1032805.
- [23] Karthik, K., Madhukesh, J.K., Kiran, S., K.V., N., Prasannakumara, B.C., Fehmi, G., Impacts of thermophoretic deposition and thermal radiation on heat and mass transfer analysis of ternary nanofluid flow across a wedge, *International Journal of Modelling and Simulation*, 2024, DOI: 10.1080/02286203.2023.2298234.





- [24] Yogeeshha, K.M., Megalamani, S.B., Gill, H.S., Umehaiah, M., Madhukesh, J.K., The physical impact of blowing, Soret and Dufour over an unsteady stretching surface immersed in a porous medium in the presence of ternary nanofluid, *Heat Transfer*, 51(7), 2022, 6961-6976.
- [25] Yadav, P.K., Yadav, N., A study on the flow of couple stress fluid in a porous curved channel, *Computers & Mathematics with Applications*, 152, 2023, 1-15
- [26] Jaiswal, S., Yadav, P.K., Physics of generalized Couette flow of immiscible fluids in anisotropic porous medium, *International Journal of Modern Physics B*, 2023, DOI: 10.1142/S0217979224503776.
- [27] Yadav, P.K., Kumar, A., El-Sapa, S., Chamkha, A.J., Impact of thermal radiation and oriented magnetic field on the flow of two immiscible fluids through porous media with different porosity, *Waves in Random and Complex Media*, 2022, DOI: 10.1080/17455030.2022.2118897.
- [28] Yadav, P.K., Verma, A.K., Analysis of the MHD flow of immiscible fluids with variable viscosity in an inclined channel, *Journal of Applied Mechanics and Technical Physics*, 64(4), 2023, 618-627.
- [29] Darvesh, A., Sánchez-Chero, M., Sánchez-Chero, J.A., Hernández, V.D.H., Guachilema, M.D.C., Reyna-Gonzalez, J.E., Influence of motile gyrotactic microorganisms over cylindrical geometry attached Cross fluid flow mathematical model, *Heat Transfer*, 52(6), 2023, 4293-4316.
- [30] Odenbach, S., Magnetic fluids-suspensions of magnetic dipoles and their magnetic control, *Journal of Physics: Condensed Matter*, 15(15), 2003, S1497.
- [31] Wang, Z., Holm, C., Müller, H.W., Boundary condition effects in the simulation study of equilibrium properties of magnetic dipolar fluids, *The Journal of Chemical Physics*, 119(1), 2003, 379-387.
- [32] Zeeshan, A., Majeed, A., Ellahi, R., Effect of magnetic dipole on viscous ferro-fluid past a stretching surface with thermal radiation, *Journal of Molecular Liquids*, 215, 2016, 549-554.
- [33] Zeeshan, A., Majeed, A., Fetecau, C., Muhammad, S., Effects on heat transfer of multiphase magnetic fluid due to circular magnetic field over a stretching surface with heat source/sink and thermal radiation, *Results in Physics*, 7, 2017, 3353-3360.
- [34] Darvesh, A., Altamirano, G.C., Sánchez-Chero, M., Sánchez-Chero, J.A., Seminario-Morales, M.V., Alvarez, M.T., Characterization of Cross nanofluid based on infinite shear rate viscosity with inclination of magnetic dipole over a three-dimensional bidirectional stretching sheet, *Heat Transfer*, 51(8), 2022, 7287-7306.
- [35] Ayub, A., Wahab, H.A., Sabir, Z., Arbi, A., A note on heat transport with the aspect of magnetic dipole and higher order chemical process for steady micropolar fluid, *Computational Overview of Fluid Structure Interaction*, 97, 2020.
- [36] Kumar, V., Madhukesh, J.K., Jyothi, A.M., Prasannakumara, B.C., Khan, M.I., Chu, Y.M., Analysis of single and multi-wall carbon nanotubes (SWCNT/MWCNT) in the flow of Maxwell nanofluid with the impact of magnetic dipole, *Computational and Theoretical Chemistry*, 1200, 2021, 113223.
- [37] Umehaiah, M., Madhukesh, J., Khan, U., Rana, S., Zaib, A., Raizah, Z., Galal, A.M., Dusty nanofluid flow through a stretching cylinder in a porous medium with the influence of the melting effect, *Processes*, 10(6), 2022, 1065.
- [38] Yadav, P.K., Verma, A.K., Analysis of immiscible Newtonian and non-Newtonian micropolar fluid flow through porous cylindrical pipe enclosing a cavity, *The European Physical Journal Plus*, 135, 2020, 1-35.
- [39] Christov, C.I., On frame indifferent formulation of the Maxwell-Cattaneo model of finite-speed heat conduction, *Mechanics Research Communications*, 36(4), 2009, 481-486.
- [40] Han, S., Zheng, L., Li, C., Zhang, X., Coupled flow and heat transfer in viscoelastic fluid with Cattaneo-Christov heat flux model, *Applied Mathematics Letters*, 38, 2014, 87-93.
- [41] Hayat, T., Khan, M. I., Farooq, M., Alsaedi, A., Waqas, M., Yasmeen, T., Impact of Cattaneo-Christov heat flux model in flow of variable thermal conductivity fluid over a variable thickened surface, *International Journal of Heat and Mass Transfer*, 99, 2016, 702-710.
- [42] Khan, M., Khan, W.A., Three-dimensional flow and heat transfer to Burgers fluid using Cattaneo-Christov heat flux model, *Journal of Molecular Liquids*, 221, 2016, 651-657.
- [43] Deo, S., Yadav, P.K., Stokes flow past a swarm of porous nanocylindrical particles enclosing a solid core, *International Journal of Mathematics and Mathematical Sciences*, 2008, 651910.
- [44] Yadav, P.K., Jaiswal, S., Puchakatla, J.Y., Yadav, M.K., Flow through membrane built up by impermeable spheroid coated with porous layer under the influence of uniform magnetic field: effect of stress jump condition, *The European Physical Journal Plus*, 136(1), 2021, 1-34.
- [45] Khan, M.S., Karim, I., Arifuzzaman, S.M., Rahman, M.M., Biswas, P., Williamson fluid flow behaviour of MHD convective-radiative Cattaneo-Christov heat flux type over a linearly stretched-surface with heat generation and thermal-diffusion, *Frontiers in Heat and Mass Transfer*, 9(1), 2017, 1-11.
- [46] Ayub, A., Asjad, M.I., Al-Malki, M.A., Khan, S., Eldin, S.M., Abd El-Rahman, M., Scrutiny of nanoscale heat transport with ion-slip and hall current on ternary MHD cross nanofluid over heated rotating geometry, *Case Studies in Thermal Engineering*, 53, 2024, 103833.
- [47] Shah, S.Z.H., Sabir, Z., Ayub, A., Rashid, A., Sadat, R., Ali, M.R., An efficient numerical scheme for solving the melting transportation of energy with time dependent Carreau nanofluid, *South African Journal of Chemical Engineering*, 47, 2024, 345-356.
- [48] Yadav, P.K., Deo, S., Yadav, M.K., Filippov, A., On hydrodynamic permeability of a membrane built up by porous deformed spheroidal particles, *Colloid Journal*, 75, 2013, 611-622.
- [49] Salawu, S., Obalalu, A., Shamshuddin, M., Nonlinear solar thermal radiation efficiency and energy optimization for magnetized hybrid Prandtl-Eyring nanofluid in aircraft, *Arabian Journal for Science and Engineering*, 48, 2022, 1-12.
- [50] Shankar, B., Yirga, Y., Unsteady heat and mass transfer in MHD flow of nanofluids over stretching sheet with a non-uniform heat source/sink, *International Journal of Mathematical, Computational, Statistical, Natural and Physical Engineering*, 7(12), 2013, 1248-1255.
- [51] Ramzan, M., Bilal, M., Chung, J.D., MHD stagnation point Cattaneo-Christov heat flux in Williamson fluid flow with homogeneous-heterogeneous reactions and convective boundary condition—A numerical approach, *Journal of Molecular Liquids*, 225, 2017, 856-862.
- [52] Kumar, K.G., Gireesha, B.J., Rudraswamy, N.G., Krishnamurthy, M.R., An unsteady flow and melting heat transfer of a nanofluid over a stretching sheet embedded in a porous medium, *International Journal of Applied Mechanics and Engineering*, 24(2), 2019, 245-258.
- [53] Upadhya, S.M., Raju, C.S.K., Saleem, S., Nonlinear unsteady convection on micro and nanofluids with Cattaneo-Christov heat flux, *Results in Physics*, 9, 2018, 779-786.
- [54] Kumar, K.A., Reddy, J.R., Sugunamma, V., Sandeep, N., MHD flow of chemically reacting Williamson fluid over a curved/flat surface with variable heat source/sink, *International Journal of Fluid Mechanics Research*, 46(5), 2019, DOI: 10.1615/InterJFluidMechRes.2018025940.
- [55] Gherieb, S., Kezzar, M., Ayub, A., Sari, M.R., Khan, U., Muhammad, T., Ali, M.R., Insight into the dynamics of slip and radiative effect on magnetohydrodynamic flow of hybrid ferroparticles over a porous deformable sheet, *ZAMM-Journal of Applied Mathematics and Mechanics/Zeitschrift für Angewandte Mathematik und Mechanik*, 2024, e202300729.
- [56] Salawu, S.O., Obalalu, A.M., Akinola, E.I., Current density and thermal propagation of electromagnetic CoFe₂O₄ and TiO₂/C₂H₆O₂+H₂O hybridized Casson nanofluids: a concentrated solar power maximization, *Results in Engineering*, 18, 2023, 101200.
- [57] Darvesh, A., Altamirano, G.C., Inclined magnetic dipole and nanoscale energy exchange with infinite shear rate viscosity of 3D radiative cross nanofluid, *Heat Transfer*, 51(4), 2022, 3166-3186.
- [58] Obalalu, A.M., Salawu, S.O., Olayemi, O.A., Ajala, O.A., Issa, K., Analysis of hydromagnetic Williamson fluid flow over an inclined stretching sheet with Hall current using Galerkin Weighted Residual Method, *Computers and Mathematics with Applications*, 146, 2023, 22-32.
- [59] Khan, N.S., Usman, A.H., Sohail, A., Hussanan, A., Shah, Q., Ullah, N., Humphries, U.W., A framework for the magnetic dipole effect on the thixotropic nanofluid flow past a continuous curved stretched surface, *Crystals*, 11(6), 2021, 645.
- [60] Al-Kouz, W., Owhaib, W., Ayub, A., Souayah, B., Hader, M., Homod, R.Z., Khan, U., Thermal proficiency of magnetized and radiative cross-ternary hybrid nanofluid flow induced by a vertical cylinder, *Open Physics*, 22(1), 2024, 20230197.
- [61] Ayub, A., Sabir, Z., Said, S.B., Baskonus, H.M., Núñez, R.A.S., Sadat, R., Ali, M.R., Analysis of auto cubic catalysis and nanoscale heat transport using the inclined magnetized Cross fluid past over the wedge, *Waves in Random and Complex Media*, 2023, DOI: 10.1080/17455030.2023.2205961.
- [62] Botmart, T., Ayub, A., Sabir, Z., Weera, W., Sadat, R., Ali, M.R., Infinite shear rate aspect of the cross-nanofluid over a cylindrical channel with activation energy and inclined magnetic dipole effects, *Waves in Random and Complex Media*, 2022, DOI: 10.1080/17455030.2022.2160028.
- [63] Ayub, A., Sabir, Z., Said, S.B., Baskonus, H.M., Sadat, R., Ali, M.R., Nature analysis of Cross fluid flow with inclined magnetic dipole, *Microsystem Technologies*, 29(5), 2023, 697-714.
- [64] Khan, S., Ayub, A., Shah, S.Z.H., Sabir, Z., Rashid, A., Shoaib, M., Ali, M.R., Analysis of inclined magnetized unsteady cross nanofluid with buoyancy effects and energy loss past over a coated disk, *Arabian Journal of Chemistry*, 16(10), 2023, 105161.



ORCID iD

A.M. Obalalu  <https://orcid.org/0000-0003-0638-5928>

Adil Darvesh  <https://orcid.org/0000-0003-4906-3072>

M. Asif Memon  <https://orcid.org/0000-0002-2608-6557>



© 2024 Shahid Chamran University of Ahvaz, Ahvaz, Iran. This article is an open access article distributed under the terms and conditions of the Creative Commons Attribution-NonCommercial 4.0 International (CC BY-NC 4.0 license) (<http://creativecommons.org/licenses/by-nc/4.0/>).

How to cite this article: Obalalu, A.M., Darvesh, A., Akindele, A.O., Phulpoto, A., Adeshola, A.D., Asif Memon, M. Analysis of Ferrohydrodynamic Interaction in Unsteady Nanofluid Flow over a Curved Stretching Sheet with Melting Heat Peripheral Conditions, *J. Appl. Comput. Mech.*, xx(x), 2024, 1–16. <https://doi.org/10.22055/JACM.2024.45853.4421>

Publisher's Note Shahid Chamran University of Ahvaz remains neutral with regard to jurisdictional claims in published maps and institutional affiliations.

